A mitotic kinesin-6, Pav-KLP, mediates interdependent cortical reorganization and spindle dynamics in *Drosophila* embryos

Patrizia Sommi[1],*, Revathi Ananthakrishnan[1], Dhanya K. Cheerambathur[1],‡, Mijung Kwon[1],§, Sandra Morales-Mulia[1],¶, Ingrid Brust-Mascher[1,2],** and Alex Mogilner[3],**,‡‡

[1]LCCB, Center for Genetics and Development, [2]Department of Molecular and Cellular Biology, and [3]Department of Neurobiology, Physiology and Behavior and Department of Mathematics, University of California at Davis, Davis, CA 95616, USA

*Present address: Department of Physiology, Human Physiology Section, University of Pavia, Pavia, 27100, Italy
‡Present address: Department of Cellular and Molecular Medicine, Ludwig Institute for Cancer Research, University of California, San Diego, La Jolla, CA 92093, USA
§Present address: Department of Pediatric Oncology, Dana-Farber Cancer Institute, Boston, MA 02115, USA
¶Present address: Instituto Nacional de Psiquiatria, Depto. Neurofarmacologia, Mexico City, 14370, Mexico
**These authors contributed equally to this work
‡‡Author for correspondence (mogilner@math.ucdavis.edu)

Summary

We investigated the role of Pav-KLP, a kinesin-6, in the coordination of spindle and cortical dynamics during mitosis in *Drosophila* embryos. In vitro, Pav-KLP behaves as a dimer. In vivo, it localizes to mitotic spindles and furrows. Inhibition of Pav-KLP causes defects in both spindle dynamics and furrow ingression, as well as causing changes in the distribution of actin and vesicles. Thus, Pav-KLP stabilizes the spindle by crosslinking interpolar microtubule bundles and contributes to actin furrow formation possibly by transporting membrane vesicles, actin and/or actin regulatory molecules along astral microtubules. Modeling suggests that furrow ingression during cellularization depends on: (1) a Pav-KLP-dependent force driving an initial slow stage of ingression; and (2) the subsequent Pav-KLP-driven transport of actin- and membrane-containing vesicles to the furrow during a fast stage of ingression. We hypothesize that Pav-KLP is a multifunctional mitotic motor that contributes both to bundling of interpolar microtubules, thus stabilizing the spindle, and to a biphasic mechanism of furrow ingression by pulling down the furrow and transporting vesicles that deliver new material to the descending furrow.

Key words: Pavarotti, Kinesin-6, Actin, Mitosis, Nuf, Vesicles

Introduction

Dynamic interactions between the mitotic spindle, the cell cortex and the plasma membrane underlie many crucial cellular phenomena. For example, during cell division, the localization of the cleavage furrow is specified by the mitotic spindle (Glotzer, 2001; Scholey et al., 2003; Odell and Foe, 2008), whereas actomyosin-based cortical contractions contribute to spindle morphogenesis (Rosenblatt et al., 2004). In addition, membrane transport to the furrow is crucial for cell-cell abscission and the completion of cytokinesis (Finger and White, 2002). Recently, it has been shown that vesicles associated with F-actin are transported on furrow microtubules (MTs) (Albertson et al., 2008). However, the underlying molecular mechanisms remain largely obscure.

Drosophila embryogenesis is amenable to the study of interactions between the spindle, cortex and membrane using genetic analysis, inhibitor microinjection and microscopy (Glover, 2005). In the *Drosophila* syncytial embryo, nuclei share the same cytoplasm and undergo 13 synchronous divisions without any intervening cytokinesis; however, following the migration of the nuclei to the embryonic surface during cycle 9, mitotic furrows form transiently around each spindle (Mazumdar and Mazumdar, 2002). The mitotic furrows grow longer during each metaphase, serving as barriers to maintain the spacing between adjacent spindles, and then regress during late anaphase and telophase. Subsequently, during interphase of cycle 14, cellularization furrows descend from the blastoderm surface to partition the nuclei into individual cells.

Many studies suggest that spindle morphogenesis, as monitored by the separation of the spindle poles, depends upon a balance of forces generated by multiple molecular motors that guide the spindle through a sequence of quiescent steady states interspersed with phases of rapid spindle-pole separation (Sharp et al., 2000; Brust-Mascher et al., 2004; Cytrynbaum et al., 2005). The mitotic furrows maintain a constant distance to the poles throughout mitosis, and perturbations of mitotic molecules can cause both spindle and cortical defects during the early mitotic cycles (Cytrynbaum et al., 2005). To test the hypothesis that this force balance reflects a dynamic relationship between the spindle and the cortex, we need to know the identity of the crucial molecules that influence the structure and dynamics of both the spindle and the cortex. It is unknown how the spindle affects cortical reorganization and, conversely, how the cortex affects spindle morphogenesis.

Both cellularization and metaphase furrow formation in the early *Drosophila* embryo are driven by the MT-dependent delivery of membrane vesicles to the furrow region (Strickland and Burgess, 2004; Riggs et al., 2003). As in conventional cytokinesis, new furrow membrane does not seem to be derived from the expansion of the pre-existing surface membrane, but rather forms through the insertion of membrane from internal stores, such as the recycling endosome (RE), Golgi or both (Lecuit and Weichaus, 2000; Sisson

et al., 2000). Actomyosin-based cortical contractions are required for basal closure at the end of cellularization (Royou et al., 2004), and it has been proposed that either F-actin or actin-regulatory molecules are delivered to the growing furrows together with membrane vesicles (Riggs et al., 2003; Cao et al., 2008).

Although the exact pathways of membrane transport remain unclear, the molecular inventories are being unraveled. Two molecules, Nuf and Rab11 (both resident proteins of the RE), are crucial for membrane trafficking and actin recruitment during furrow formation (Riggs et al., 2003; Riggs et al., 2007). Rab11 is a small GTPase whose activity is required for the budding of vesicles from the RE (Ullrich et al., 1996). Microinjection of a dominant-negative Rab11 construct before cellularization leads to defects in membrane addition and furrow morphology that are very similar to the defects seen in Nuclear fallout (*nuf*) mutants (Rothwell et al., 1998; Rothwell et al., 1999; Pelissier et al., 2003; Riggs et al., 2003), suggesting that these two proteins are components of a common pathway. Nuf is a member of the Arf family of small GTPases; it binds Rab11 (Hickson et al., 2003) and participates in trafficking of recycled vesicles to the plasma membrane and in actin assembly (Rothwell et al., 1999; Riggs et al., 2003; Riggs et al., 2007).

The observation that membrane-vesicle recruitment is crucial for furrow growth raises questions about the mechanism of vesicle delivery to the furrow, and the identity of the responsible cytoskeletal motors and tracks. A number of studies are consistent with the notion that this transport is driven along astral MTs by the MT plus-end-directed motor kinesin-6 (Pav-KLP in *Drosophila*) (Adams et al., 1998; Foe et al., 2000; Minestrini et al., 2003; Cytrynbaum et al., 2005). Pav-KLP plays an important role in mediating spindle-cortical interactions in mitosis and cytokinesis (Adams et al., 1998; Somma et al., 2002).

During telophase, Pav-KLP localizes to the spindle midbody, where interpolar MT (ipMT) plus ends are localized, and promotes MT bundling (Adams et al., 1998; Minestrini et al., 2003; Nislow et al., 1992; Mishima et al., 2004; Goshima and Vale, 2005). Pav-KLP is proposed to transport Polo kinase to the central spindle (Adams et al., 1998; Glover, 2005), and defects in Pav-KLP accumulation at the central spindle cause contractile-ring defects and the inhibition of furrow ingression (Adams et al., 1998; Somma et al., 2002; Minestrini et al., 2003). Pav-KLP is also involved in assembly of the actomyosin ring through the formation of the centralspindlin complex with the Rho-GTPase-activating protein RacGap50C and the Rho-GTP-exchanging factor (RhoGEF) Pebble, which localizes to the equatorial cortex and activates Rho1 (Somers and Saint, 2003). Minestrini et al. proposed that the role of Pav-KLP is to transport elements of the actomyosin cytoskeleton to plus ends of astral MTs in the equatorial region of the cell to permit cleavage-ring formation (Minestrini et al., 2003). In addition, Pav-KLP-driven membrane traffic to the cell surface could contribute to the dynamics of cortical actin and of the overlying cell membrane in the embryo (Albertson et al., 2005). Other kinesin-6-family motors are key regulators of mitosis and cytokinesis (Neef et al., 2006); in particular, they participate in stabilizing the equatorial region of the metaphase spindle (Colombié et al., 2008) and, as part of the centralspindlin complex, are required in central-spindle assembly and cytokinesis (Glover et al., 2008; Odell and Foe, 2008). However, the role of Pav-KLP in early mitosis in *Drosophila* syncytial embryos has not been explored.

In the current study, we investigated the role of Pav-KLP in spindle and furrow dynamics in the *Drosophila* syncytium using experimental perturbations and quantitative modeling. We hypothesize that Pav-KLP mediates cortical-spindle interactions by: (1) stabilizing the spindle and coupling spindle morphogenesis with furrow growth, and (2) transporting membrane vesicles and possibly actin and/or actin regulatory molecules along astral MTs to build the mitotic and cellularization furrows. These interactions might be complemented by feedback from the furrows where dynein generates forces to pull the spindle poles apart. In addition, Pav-KLP can contribute to furrow dynamics by pulling the furrows down along the 'inverted basket' of astral MTs. We propose that biphasic furrow ingression during cellularization depends on a Pav-KLP-generated force pulling down the furrows during the initial slow stage, followed by Pav-KLP-driven vesicle delivery to the ingressing furrows during the subsequent fast stage.

Results

Pav-KLP localizes to the embryonic mitotic spindles and cortex

We used time-lapse confocal fluorescence microscopy of *Drosophila* embryos expressing GFP–Pav-KLP injected with Rhodamine-tubulin to study the distribution of Pav-KLP. In the syncytial embryo, Pav-KLP localized to the spindle as well as to the cortices surrounding interphase nuclei and mitotic spindles (Fig. 1A), which is in agreement with previous observations (Minestrini et al., 2003). In addition to the localization of Pav-KLP on ipMTs and the midbody during anaphase and telophase, we also observed Pav-KLP on MTs that extend from the centrosomes towards the cortex close to the midbody (Fig. 1B). Although cytokinesis is absent in the syncytium, these Pav-KLP-positive MTs contacting the cortex can be compared to the peripheral MTs in *Drosophila* spermatocytes, at which the centralspindlin complex has been shown to localize and which are proposed to be involved in initiating the cleavage furrow (Inoue et al., 2004). During later embryonic cycles, which exhibit a conventional cytokinesis, Pav-KLP exhibited a similar distribution: it accumulated both on the spindle and at the cortex, marking the position of the future contractile ring (Fig. 1C). Immunofluorescence performed using the antibody we generated against the Pav-KLP tail confirmed the distribution observed using GFP–Pav-KLP embryos and showed that the cortical pool of Pav-KLP displays a striking colocalization with actin at the mitotic furrows (Fig. 1D).

Pav-KLP is required for normal spindle morphogenesis

To study the role of Pav-KLP in the syncytial embryo, we generated an antibody against the Pav-KLP tail (see Materials and Methods); this antibody reacted specifically and with high affinity with the *Drosophila* syncytial blastoderm cytosol at the predicted molecular mass for Pav-KLP (supplementary material Fig. S1A).

We microinjected this antibody into GFP–Pav-KLP-expressing embryos and compared the localization of GFP–Pav-KLP with and without antibody inhibition (Fig. 2A). Upon injection of anti-Pav-KLP antibody, there was a strong decrease in GFP–Pav-KLP fluorescence intensity at the spindle and cortex (Fig. 2A, compare a and b with c and d, respectively) even though GFP–Pav-KLP was not completely displaced from the cortex. The results suggest that Pav-KLP recruitment to its presumptive sites of function has been perturbed and, although the antibody has not been proven to block Pav-KLP catalytic activity, antibody injection allows us to study the role of Pav-KLP.

Previous studies have shown that Pav-KLP is involved in spindle-midzone organization (Adams et al., 1998; Somma et al.,
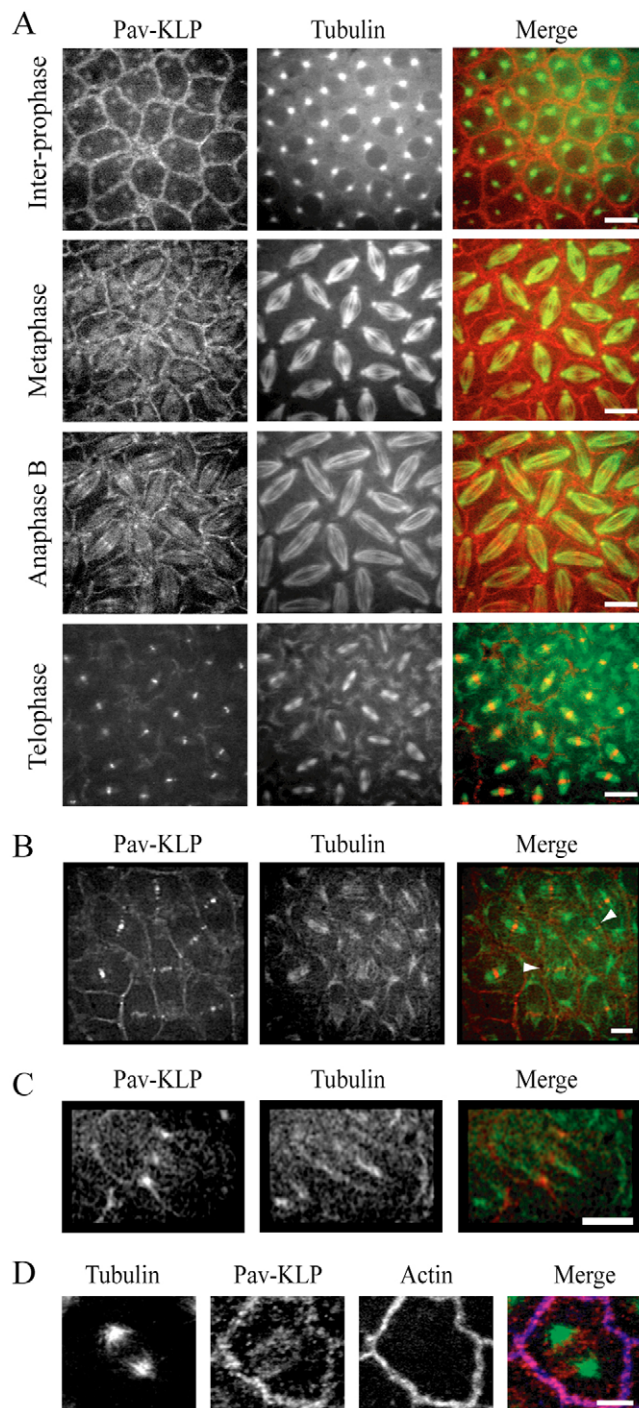
Fig. 1. Pav-KLP localization. (**A**) In the syncytial embryo, GFP–Pav-KLP localizes to the centrosomes and the cortex before NEB. After NEB, GFP–Pav-KLP also localizes to spindle microtubules. It concentrates at the equator during anaphase B and the midbody during telophase. In the merged image, GFP–Pav-KLP is red and tubulin green. Scale bars: 10 μm. (**B**) GFP–Pav-KLP distribution during early telophase. Pav-KLP (red) is mainly focused in the narrow band of MTs (green) engaged in forming the spindle midbody ('internal' MTs), although a small fraction is on MTs positioned outside the spindle midbody and contacting the cortex ('peripheral' MTs, arrowheads). Scale bar: 10 μm. (**C**) Initial stages of furrow ingression in GFP–Pav-KLP post-cellularized embryos. Pav-KLP (red) accumulates on the spindle (green) at the site of furrow ingression. Scale bar: 10 μm. (**D**) Immunolocalization of Pav-KLP in the syncytium. Pav-KLP (red) at the cortex colocalizes with actin (blue). Regions of colocalization are pink. Tubulin is shown in green. Scale bar: 2 μm.

elongate after metaphase (region 'a' in Fig. 2B,C), and milder defects away from the injection site, where spindles displayed normal dynamics but had disorganized midbodies during telophase (region 'b' in Fig. 2B,C). Analysis of defective spindle morphogenesis and Pav-KLP displacement showed a correlation between the two: that is, spindles form and complete mitosis in regions where some protein is left (i.e. distal to the injection site), whereas spindles void of detectable Pav-KLP (i.e. proximal to the injection site) fail to complete mitosis (supplementary material Fig. S1). Spindles in the region exhibiting a mild phenotype consistently developed the severe phenotype during the subsequent mitosis.

The phenotypes most commonly observed were a delay in nuclear-envelope breakdown (NEB; Fig. 2B, region 'a'), defects in pole-pole separation resulting in spindle collapse or short spindles (Fig. 2D) and disorganized or absent telophase midbodies, which were sometimes associated with collapsed or fused daughter nuclei (Fig. 2D). Sometimes, adjacent spindles were observed to form interconnections, suggesting a disruption of the mitotic furrows that normally keep the spindles physically separate within the syncytium. Similar spindle defects were observed in Pav-KLP RNAi-treated S2 cells (Fig. 2E), supporting the idea that the mitotic defects observed in the syncytium upon injection of anti-Pav-KLP antibody are due to specific Pav-KLP inhibition.

The spindle collapse induced by anti-Pav-KLP occurred in metaphase, later than that observed after inhibition of the bipolar kinesin KLP61F (Sharp et al., 2000; Brust-Mascher et al., 2009), which consistently caused collapse at the onset of the prometaphase spindle elongation (Fig. 2C), suggesting that Pav-KLP function is necessary to maintain pole-pole spacing after spindle assembly. Defects in spindle morphogenesis were accompanied by defects in chromosome segregation and kinetochore movement, observed when Pav-KLP was inhibited in GFP-Histone- or GFP-ROD (Rough deal; a kinetochore protein)-expressing embryos (supplementary material Fig. S2). Pav-KLP inhibition in GFP-ROD-expressing embryos led to a decrease in the rate of kinetochore-to-pole movement from 0.1±0.02 μm/second in control to 0.06±0.02 μm/second in anti-Pav-KLP-injected embryos.

In summary, our data suggest that, in the *Drosophila* syncytium, Pav-KLP is involved in stabilizing the spindle structure in order to ensure proper spindle assembly and function, and that Pav-KLP plays essential roles in the maintenance of pole-pole spacing and in the prevention of spindle collapse in metaphase, possibly by crosslinking ipMTs.

2002; Minestrini et al., 2003). Therefore, we looked at the role of Pav-KLP in spindle assembly in syncytial embryos. We performed real-time analysis of spindle morphogenesis after injection of the anti-Pav-KLP antibody into GFP-tubulin-expressing embryos. Microinjection of anti Pav-KLP generated a concentration gradient of antibody and thus led to Pav-KLP inhibition levels that result in a gradient of phenotypes with the most severe defects occurring proximal to the injection site (Fig. 2B; supplementary material Fig. S1). Spindle-pole separation kinetics after Pav-KLP inhibition exhibited severe defects near the injection site, where spindles either collapsed or did not
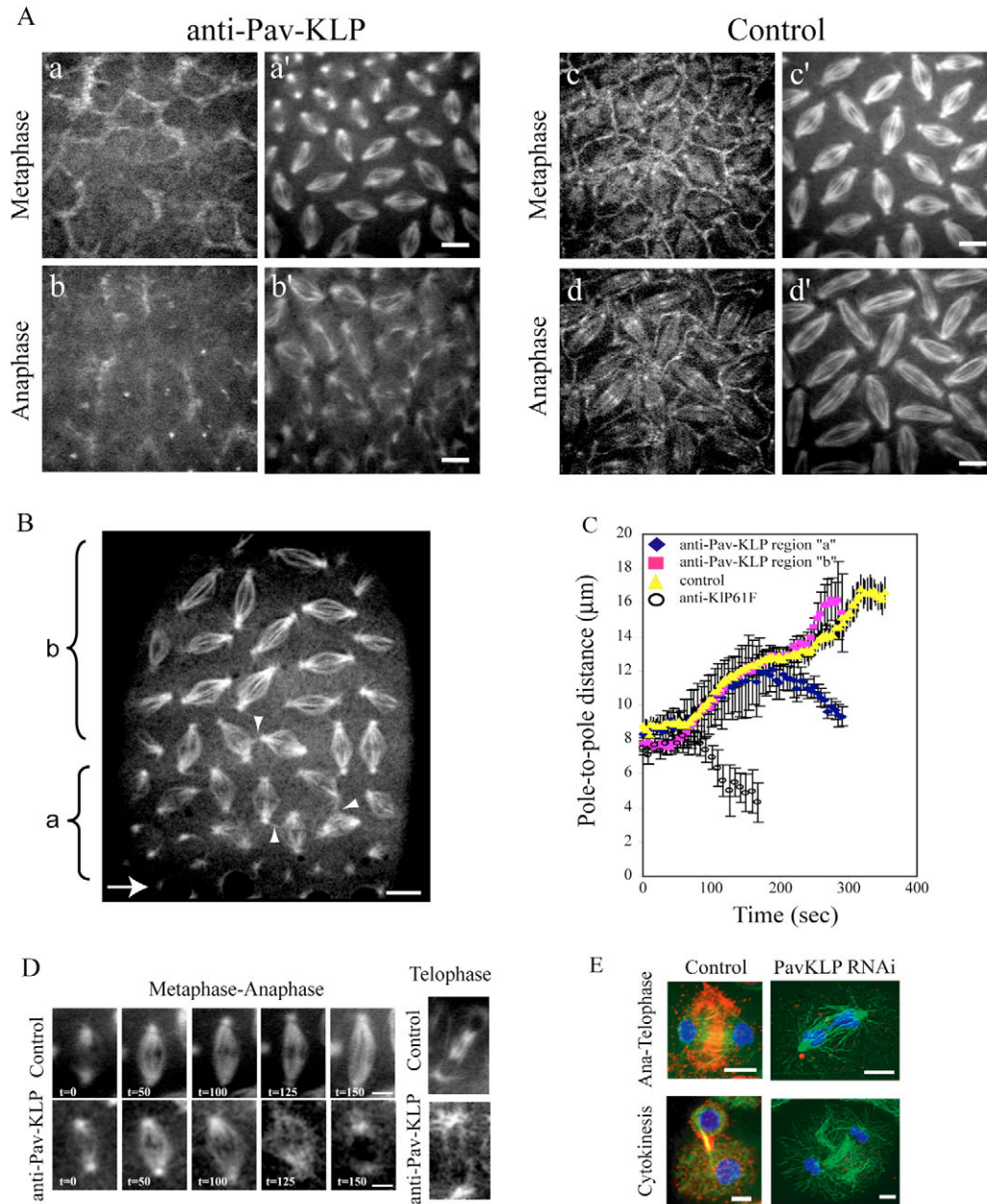
Fig. 2. Effect of Pav-KLP inhibition on spindle morphogenesis. (**A**) Anti-Pav-KLP antibody injected into GFP–Pav-KLP-expressing embryos (previously injected with Rhodamine-tubulin) leads to Pav-KLP displacement (a-b). Compared with control, Pav-KLP inhibition causes a decrease in GFP signal in metaphase (a vs c) and anaphase (b vs d) both on the spindle and at the cortex. The decrease in GFP signal is paired with defects in spindle organization (a′ and b′ vs c′ and d′, respectively). Scale bars: 5 μm. (**B**) Injection of anti-Pav-KLP antibody into GFP-tubulin-expressing embryos (arrow shows site of injection) causes a gradient of defects, with the more severe ones adjacent to the injection site (region 'a') and the less severe ones more distal (region 'b'). Interconnected adjacent spindles are shown by arrowheads. Scale bar: 10 μm. (**C**) Plot of pole-to-pole distances in spindles from regions 'a' and 'b' in B within the embryo (blue and red, respectively, in the graph). Control is yellow. For comparison, we show pole-to-pole distance measured in anti-KLP61F-injected embryos (circles); spindles in these embryos collapse at the onset of the prometaphase-to-metaphase transition. (**D**) Examples of spindle defects. Left panels: spindle in region 'a' in B does not elongate during anaphase B. Right: spindle has no midbody during telophase. Scale bars: 5 μm. (**E**) S2 cells treated with dsRNA for *Pav-KLP*. dsRNA-treated cell in late anaphase (top) shows disorganized MTs and defects in chromosome segregation. dsRNA-treated cell in cytokinesis (bottom) lacks the compact midbody seen in control cells. Pav-KLP, red; tubulin, green; DNA, blue. Scale bars: 5 μm.

Pav-KLP behaves as a dimer

Because our observations in vivo suggest that Pav-KLP associates with MTs and is involved in spindle assembly possibly via MT crosslinking, we investigated the oligomeric status of Pav-KLP and its interaction with MTs in vitro to get a better understanding of its molecular mechanism. To determine the subunit composition of Pav-KLP in *Drosophila*, we performed hydrodynamic assays with embryonic extract and used anti-Pav-KLP antibody to probe for the presence of Pav-KLP. We observed that Pav-KLP co-sedimented with MTs in the presence of either AMP-PNP (a
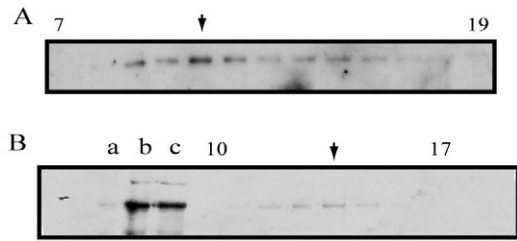
Fig. 3. Biochemical analysis of native Pav-KLP from *Drosophila* embryo extract. (**A**) Fractions 7-19 from 5-20% sucrose density gradient probed by anti-Pav-KLP immunoblotting. The predominant peak (arrow) corresponds to the dimer form. There is a second peak (arrow in B), which could correspond to a monomeric form of Pav-KLP, subject to future investigation. (**B**) Immunoblotting of embryo MTs and gel filtration fractions probed with anti-Pav-KLP. Lanes: a, *Drosophila* high-speed supernatant (HSS); b, AMPPMP-MT pellet; c, ATP plus 300 mM KCl eluate of AMPPNP-MTs; gel filtration fractions 10-17 containing Pav-KLP.

nonhydrolyzable ATP analog) or ATP, and, based on the Stokes radius of 7.6 nm and sedimentation coefficient of 5.8 S (Fig. 3), we estimated that Pav-KLP is a dimer with a native molecular mass of about 200 kDa.

Pav-KLP is required for normal furrow growth

The observation that connections formed between adjacent spindles in the absence of Pav-KLP suggests that the inhibition of Pav-KLP affects furrow and actin organization in the syncytial embryos. To visualize actin dynamics, we injected Rhodamine-actin with or without anti-Pav-KLP antibody into syncytial embryos expressing GFP-tubulin. In wild-type embryos, actin was organized into caps, which lay just above each spindle, and mitotic furrows, which surround each spindle and grow longer during each metaphase presumably to serve as a barrier between adjacent spindles (Fig. 4A,B). Inhibition of Pav-KLP function disrupted the localization of F-actin to the furrows but not F-actin distribution in the actin caps. Mitotic furrows did not form in the absence of Pav-KLP (Fig. 4A-C). We propose that Pav-KLP, which has a striking colocalization with this actin-based structure (Fig. 1D), is involved
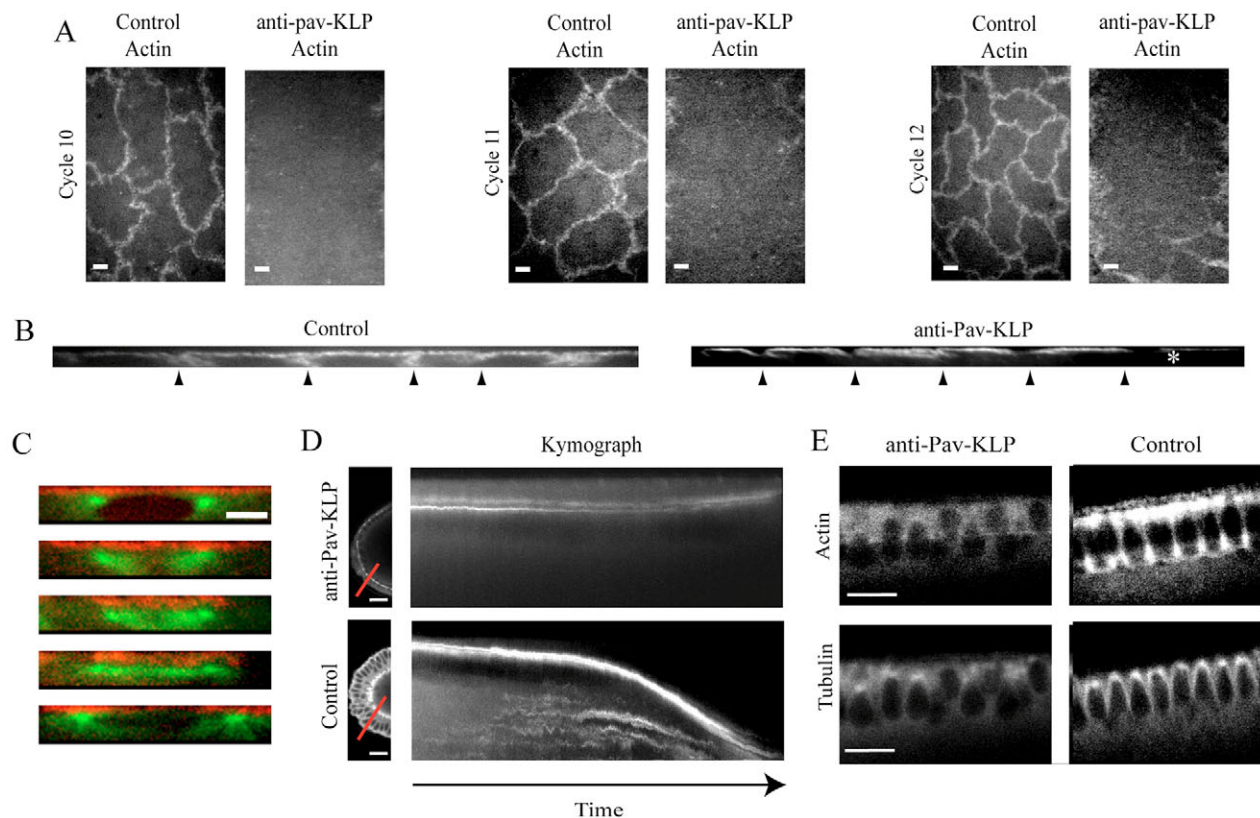

Fig. 4. Effect of Pav-KLP inhibition on furrow elongation and F-actin organization. (**A**) Single plane top views of syncytial embryos show defects in actin distribution within mitotic furrows in three cycles (10, 11 and 12). Scale bars: 5 μm. (**B**) Actin distribution in sections taken perpendicular to the embryo surface within antibody-injected and control embryos show significant differences in furrow length. Antibody injection site is at the right of the image (asterisk). Arrowheads point to furrow positions. (**C**) Furrow growth is inhibited after Pav-KLP inhibition. A representative spindle shows no furrow growth from interphase-prophase (top) to telophase (bottom). Tubulin, green; actin, red. Scale bar: 5 μm. Images are shown at 50-second intervals. (**D**) Sagittal view (left) and kymograph of cellularization in embryos expressing GFP-tagged myosin-II light chain with or without anti-Pav-KLP antibody. Scale bars: 20 μm. Kymographs taken along the red line during cellularization show movement of the growing furrow tips (time course = 50 minutes). Anti-Pav-KLP antibody injection (top) prevents the furrow ingression seen in controls (bottom). (**E**) GFP-tubulin-expressing embryo injected with anti-Pav-KLP antibody and Rhodamine-actin. Decreased actin recruitment (top) and less organized MTs (bottom) are observed during cellularization in Pav-KLP-inhibited embryos (left). After inhibition, nuclei are misaligned and some fall out. Scale bars: 20 μm.

in furrow elongation. The distribution of actin in the actin caps was not significantly affected, suggesting that Pav-KLP activity specifically influences actin distribution at the furrows possibly by transporting actin itself or actin accessory proteins.

Pav-KLP is required for furrow growth during cellularization

To explore the idea that Pav-KLP is required for furrow and/or actin morphogenesis in later mitotic cycles, we investigated the role of Pav-KLP during cellularization, which resembles conventional cytokinesis (Foe and Alberts, 1983; Edgar et al., 1987; Foe et al., 2000). In the *Drosophila* embryo, cellularization occurs after cycle 13 and involves the descent of the furrow canal beyond the nuclei to form the columnar epithelium. The furrow growth during cellularization is biphasic with an initial slow phase, during which the membrane reaches the base of the nuclei, and a second fast phase, in which a higher rate of growth is followed by fusion of the membrane at the base to form separate units (Foe et al., 1983). The furrow canal has a similar organization to the metaphase furrows and both require a dramatic reorganization of actin and myosin (Warn et al., 1980; Warn and Magrath, 1983; Young et al., 1991).

In order to probe the effect of Pav-KLP on furrow growth during cellularization, embryos were injected with the antibody at the end of cycle 13. In Pav-KLP-inhibited embryos, myosin still localized to the tips of the furrow canals, and so we used GFP-tagged myosin-II light chain (spaghetti squash *Drosophila* protein) as a marker to follow the dynamics of the furrow canal (Young et al., 1991). When Pav-KLP activity was blocked, defects in furrow-canal growth were clearly visible: furrows were only a few μm long even at the time when the cellularization front in control embryos would be at the base of the nuclei (Fig. 4D). Subsequently, we monitored the recruitment and distribution of actin in these few-μm-long furrows in the Pav-KLP-inhibited embryos by co-injecting the antibody with Rhodamine-actin into GFP-tubulin-expressing embryos. In control embryos, actin localizes to the growing furrows and concentrates at their tips. In addition, it associates with apical cap surfaces (Fig. 4E) (Warn and Robert-Nicoud, 1990). When Pav-KLP was inhibited, although actin was recruited to these small furrows, there was a strikingly reduced amount of actin at the tips (Fig. 4E, Actin). These defects in furrow-canal growth were, in fact, similar to those observed after injection of cytochalasin or colchicine at the onset of cellularization (Royou et al., 2004), suggesting that cytoskeletal structures and associated proteins are required for the growth and organization of furrow canals.

In Pav-KLP-inhibited embryos we also observed defects in MT and nuclear organization at the cellularization stage. In wild-type embryos, MTs distributed around the nucleus to form an envelope with an inverted-basket-shaped structure, whereas, in Pav-KLP-inhibited embryos, this distribution was not clearly visible (Fig. 4E). This phenotype could be due to a direct effect on MTs, a disorganized or diminished number of MTs, and/or less crosslinked MTs that result from loss of function of Pav-KLP. In addition, in the absence of Pav-KLP activity we found that nuclei were misaligned and, in some cases, they displayed the 'fall-out' phenotype.

Furrow ingression and plasma-membrane addition during cellularization were shown to be coupled events (Strickland and Burgess, 2004; Riggs et al., 2003); therefore, the inhibition of furrow ingression is probably accompanied by a reduction in the invagination of the plasma membrane (Riggs et al., 2003; Sisson et al., 2000). To monitor new membrane addition along the growing furrow after Pav-KLP inhibition, we injected a membrane marker [Alexa-Fluor-647-conjugated wheat germ agglutinin (WGA)] into the perivitellin space in GFP-tubulin-expressing embryos at the beginning of cellularization. When the addition of membrane was monitored in control GFP-tubulin embryos, insertion of the fluorescent marker was observed along the entire growing furrow. When Pav-KLP activity was blocked, a reduction of plasma-membrane growth was observed (supplementary material Fig. S3).

Pav-KLP is required for proper localization of Nuf

Because the functional disruption of proteins involved in membrane addition and actin remodeling, such as Rab11, Lava lamp, Nuf and RhoGEF, affect plasma-membrane invagination and furrow growth (Sullivan et al., 1993; Rothwell et al., 1998; Rothwell et al., 1999; Zhang et al., 2000; Sisson et al., 2000; Pelissier et al., 2003; Riggs et al., 2003; Barmchi et al., 2005; Papoulas et al., 2005), we considered the possibility that Pav-KLP is involved in membrane-vesicle delivery to the furrows. To study the effect of Pav-KLP inhibition on Nuf, which has been shown to be important for proper actin localization (Rothwell et al., 1998; Riggs et al., 2003), we injected anti-Pav-KLP antibody into syncytial embryos expressing GFP-Nuf. We observed a clear change in Nuf distribution and movement (Fig. 5). In control embryos, during prophase, Nuf accumulates around the centrosomes and moves radially outwards. Fig. 5A shows projections of time-lapse movies acquired in the absence and presence of anti-Pav-KLP antibody. In controls, the projection results in a large area occupied by Nuf, whereas the projection after Pav-KLP inhibition has a small area occupied by Nuf. There is also a decrease in the amount of Nuf (Fig. 5A, time 0); however, the decrease in the projection is even larger, indicating less movement. This is also evident in linescans (Fig. 5C), and kymographs (Fig. 5D), in which Nuf has a tighter distribution around the nucleus, covering an area around each centrosome about six times smaller than in controls (Fig. 5C). After NEB, Nuf redistributes around the spindle (Fig. 5B). Pav-KLP inhibition caused a severe reduction in Nuf localization and its movement around the spindle periphery (Fig. 5B)

Quantitative model of Pav-KLP-driven furrow growth during cellularization

On the basis of the above experimental results, we hypothesize that Pav-KLP delivers membrane vesicles, and possibly F-actin associated with them, to the furrow, and that this transport is the limiting factor for furrow ingression. To test this hypothesis, we developed a mathematical model (Fig. 6A; supplementary material Fig. S4) in which the vesicles diffuse in the cytoplasm, attach to astral MTs, are transported along these MTs by Pav-KLP towards MT plus ends, and detach from the MTs. We assume that the vesicles merge with the growing furrows rapidly whenever they reach the MT plus ends that are in physical contact with the furrows (inset 1 in Fig. 6A). The model is illustrated in Fig. 6A and consists of the following diffusion-drift-reaction equations:

$$\frac{\partial C_D}{\partial t} = D\left[\frac{\partial^2 C_D}{\partial x^2} + \frac{\partial^2 C_D}{\partial y^2}\right] - \left(k_{att} \times C_D\right) + \left(k_{det} \times C_{MT}\right), \quad (1)$$

$$\frac{\partial C_{MT}}{\partial t} = -\left[\frac{\partial(V_x \times C_{MT})}{\partial x}\right] - \left[\frac{\partial(V_y \times C_{MT})}{\partial y}\right] + \left(k_{att} \times C_D\right) - \left(k_{det} \times C_{MT}\right), \quad (2)$$
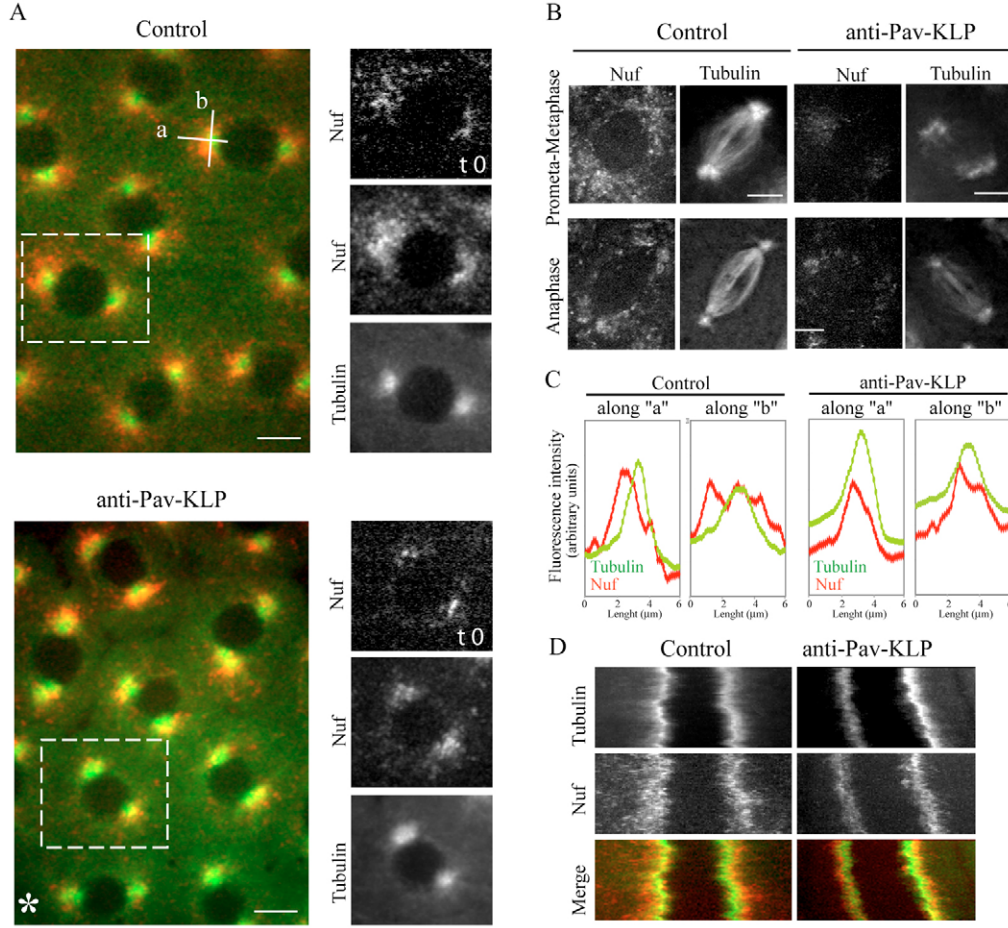
Fig. 5. Effect of Pav-KLP inhibition on Nuf distribution. GFP-Nuf-expressing embryos were injected with anti-Pav-KLP antibody and Rhodamine-tubulin. To obtain a better view of Nuf distribution over time, consecutive images are projected onto a single one. (**A**) Nuf distribution (red) around the centrosomes (tubulin, green) during prophase in a projection of images recorded every 2 seconds for a total of 50 seconds. The distribution of Nuf at t=0 is shown on the right for a single spindle (boxed area). After Pav-KLP inhibition, the amount of Nuf around the centrosomes is reduced (compare frames at t=0) and Nuf stays closer to the centrosome (compare projections over time). Asterisk marks the site of antibody injection, where defects are more severe. Scale bars: 5 μm. (**B**) Nuf distribution for different stages of mitosis. Each image is a time projection of 30 (prometaphase-metaphase) and 15 (anaphase) images taken every 0.5 seconds. The projection for Rhodamine-tubulin is used as a reference for spindle movement. Pav-KLP inhibition reduces the amount of Nuf and changes its localization. Scale bars: 5 μm. (**C**) Linescans showing tubulin and Nuf distribution in control and anti-Pav-KLP antibody injected embryos along lines 'a' and 'b' oriented as shown in A. The extension of Nuf around the centrosome is reduced after Pav-KLP inhibition, from 2.85±0.44 μm along 'a' and 6.7±0.87 μm along 'b' in control to 1±0.28 μm along 'a' and 2.9±0.7 μm along 'b' in inhibited embryos. (**D**) Kymograph of Nuf and tubulin during inter-prophase, showing that Nuf (red in merge) is less mobile and stays closer to the centrosome (green in merge) when Pav-KLP is inhibited.

where C_D and C_{MT} are the concentrations of vesicles diffusing in the cytoplasm and transported towards MT plus ends, respectively; D is the diffusion coefficient; V_x and V_y are x- and y-components of the transport velocity, respectively; and k_{att} and k_{det} are attachment and detachment rates, respectively. The attachment rate:

$$k_{att} = k_{att}^0 \left(L / r \right) \exp\left[-r / L \right] , \qquad (3)$$

is proportional to the local length density of the MTs, which decreases exponentially with the distance from the centrosome:

$$r = \sqrt{\left(x - 3\right)^2 + \left(y - 2\right)^2} , \qquad (4)$$

where L is the average MT length. The centrosome is located at (x,y)=(3,2); length units are micrometers. The transport speed, v, is constant and equal to the Pav-KLP gliding rate; the corresponding velocity direction field is determined locally by astral-MT orientation. If the astral MTs emanated radially from the centrosome to the furrows, the velocity field could be described with the formula:

$$V_x = v\left(x - 3\right) / \sqrt{\left(x - 3\right)^2 + \left(y - 2\right)^2} ,$$

$$V_y = v\left(y - 2\right) / \sqrt{\left(x - 3\right)^2 + \left(y - 2\right)^2} . \qquad (5)$$

Because the MTs are not perfectly radial but curve slightly in an 'inverted-basket' configuration, we introduce a small correction to the velocity:

$$V_x = v\left(x - 3\right) / \sqrt{\left(x - 3\right)^2 + 1.44\left(y - 2\right)^2} ,$$

$$V_y = v\left(y - 2\right) / \sqrt{\left(x - 3\right)^2 + 1.44\left(y - 2\right)^2} . \qquad (6)$$

The solution of these equations gives the local influx of vesicles deposited into the furrow $\alpha(y)$ along its entire length. Assuming that the furrow growth is proportional to this influx (the furrow extends by a small increment as soon as a vesicle merges with its side, see inset 2 in Fig. 6A), we find the furrow length, l, by solving the equation:

$$\frac{dl}{dt} = k \int_0^l \alpha(y) dy , \qquad (7)$$

where k represents the furrow-length increment per unit of vesicle flux.

We solved the model equations as described in the Materials and Methods. The model predicted that the furrow growth rate is not sensitive to the diffusion of the vesicles, their attachment and detachment rates, and average MT length, but it is very sensitive

to the gliding speed of Pav-KLP. The simulations demonstrated that deposition of vesicles at the furrow tip only does not fit the experimental data (supplementary material Fig. S5). Allowing vesicle deposition all along the length of the furrow fits the second, fast stage of furrow growth well (supplementary material Fig. S5). However, it does not fit the first, slow stage because initially, when the furrow is short, very few MT plus ends contact it, and too few vesicles are delivered to fuse with it.

Interestingly, Fullilove and Jacobson found that the existing microprojections or wrinkles in the membrane are not sufficient for the entire process of cellularization but are enough for the slow phase (Fullilove and Jacobson, 1971). Therefore, we assume that, in the first, slow stage, the furrows grow by the unfolding and pulling down of the apical membrane. We hypothesize that the force needed to pull down the existing membrane folds can be generated by Pav-KLP motors that are associated with the furrow
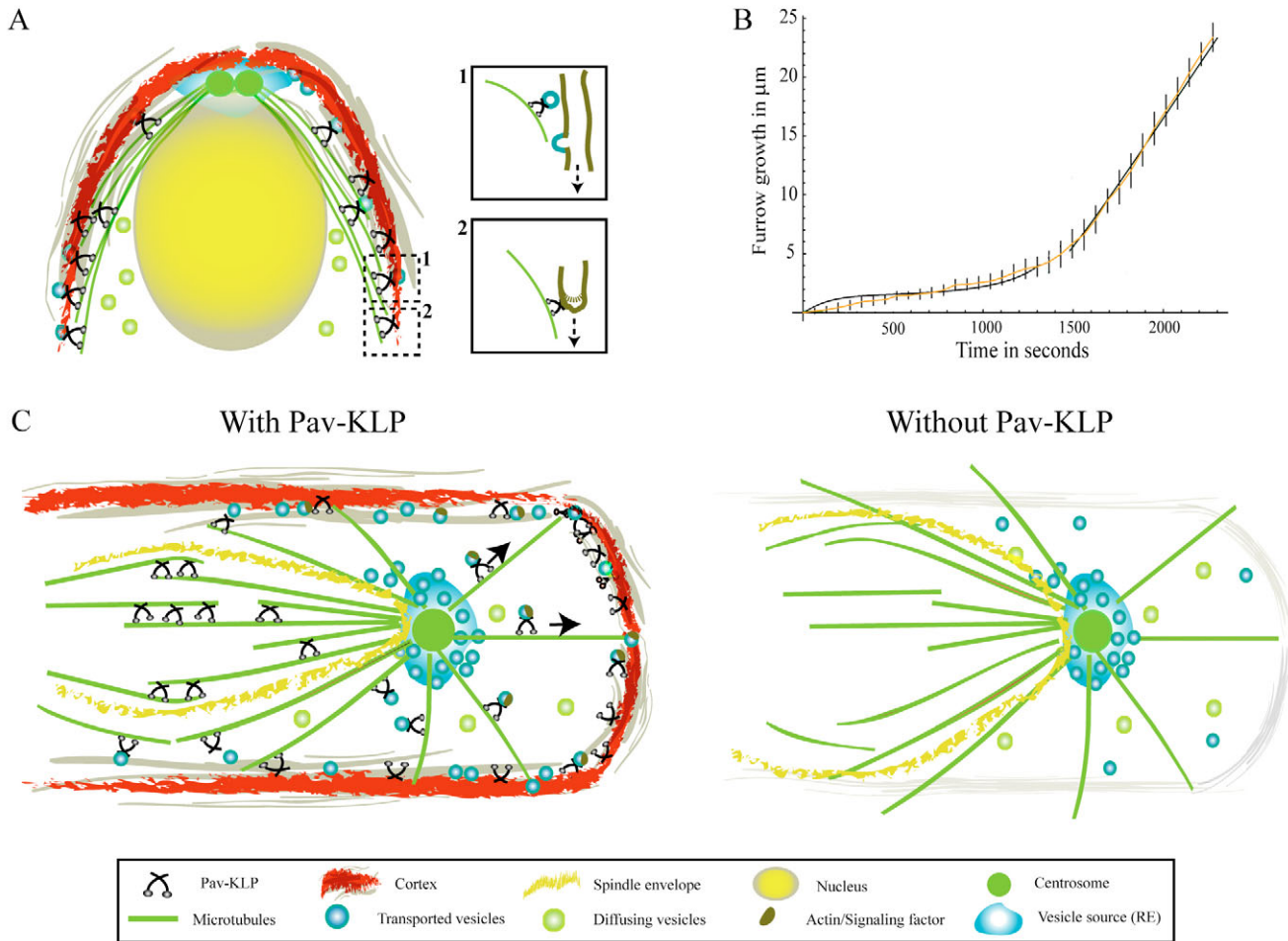

Fig. 6. Model for Pav-KLP function. (**A**) Qualitative model of furrow growth during cellularization: membrane vesicles originate near the centrosomes, diffuse through the cytoplasm, are transported by Pav-KLP on astral MTs and, upon reaching the furrow, are instantly fused laterally with it (inset 1). Pav-KLP bound to the furrow at the tip moves towards the MT plus end, pulling the furrow down (inset 2). (**B**) Model prediction for the furrow length as a function of time (two black curves). At early times the curve is derived from solving the membrane-unfolding equations; at later times the curve is derived from solving the vesicle-transport equations. These curves fit the experimental data (orange). Bars show experimental errors. (**C**) Pav-KLP functions on a single spindle in the syncytium. The cartoon shows a top view of a single spindle surrounded by the mitotic furrow. Inside the spindle envelope (yellow), Pav-KLP crosslinks ipMTs and helps stabilize the overlapping MTs in the central-spindle region; outside the spindle envelope, Pav-KLP localizes on the astral MTs, moves towards the cortex and promotes furrow growth (perpendicular to the plane shown) by transporting actin, vesicles or signaling factors to the cortex. In the absence of Pav-KLP (right), ipMTs inside the spindle envelope are not bundled and the spindle loses its shape; whereas outside the spindle envelope, loss of Pav-KLP causes defects in actin distribution, inhibiting the growth of the mitotic furrows.

tip and move towards the plus end of MTs, leading to growth past the tip (inset 2 in Fig. 6A). After the pre-existing membrane has been pulled down, furrow elongation continues by vesicle insertion.

To quantify this idea, we used a model (Herant et al., 2005) according to which there is equilibrium between unwrinkled (stretched into the furrow, l_u) and wrinkled (folded, not contributing to the furrow, l_w) membrane lengths governed by the equations:

$$\frac{dl_u}{dt} = k_+ l_w - k_- l_u$$

$$\frac{dl_w}{dt} = k_- l_u - k_+ l_w \; , \tag{8}$$

where k_+ and k_- are the rates at which the membrane folds become unfolded and the furrow membrane becomes wrinkled, respectively, by actin-dependent processes. We solve these equations assuming that, initially, there is an equilibrium and then the motor-pulling force increases parameter k_+ and decreases parameter k_- and that, initially, about half the membrane is wrinkled (Fullilove and Jacobson, 1971). By adjusting the parameters k_+ and k_-, we were able to fit the experimental data for the slow phase of furrow growth (supplementary material Fig. S6F).

This combined model fits both stages of the furrow growth quantitatively (Fig. 6B), so that the furrow grows by membrane unfolding during the first slow phase and by vesicle insertion during the second fast phase. Significantly, the experimental inhibition of Pav-KLP function affects both the slow and the fast furrow-growth stages (Fig. 4D), so we hypothesize that Pav-KLP is both (1) the force generator that is responsible for pulling down the furrow and unfolding the membrane, and (2) the vesicle transporter that delivers new cortical actin and membrane material to the ingressing furrow.

Discussion

Previous work has shown that the *Drosophila* kinesin-6, Pav-KLP, plays important roles in coordinating spindle and cortical dynamics by promoting spindle-midzone organization, contractile-ring formation and cleavage-furrow growth (Adams et al., 1998; Somma et al., 2002; Minestrini et al., 2003). Although the role of Pav-KLP in conventional cytokinesis has been well studied, little is known about Pav-KLP function in early *Drosophila* embryos, in which mitosis and cytokinesis are adapted for rapid cycles (Civelekoglu-Scholey et al., 2006). The aim of this study was to investigate the role of Pav-KLP in the syncytium, in which extremely dynamic interdependent mitotic spindles and furrows reorganize every 10-15 minutes. We demonstrate that Pav-KLP, a MT-bundling dimer, stabilizes the mitotic spindle by bundling ipMTs and, at the same time, promotes the growth of mitotic and cellularization furrows.

We observed that Pav-KLP is localized on the spindle and at the cortex, and we suggest that it performs distinct roles there (Fig. 6C). On the spindle, Pav-KLP colocalizes with MTs and is involved in spindle organization: its inhibition generates defects in pole-pole separation. Various degrees of inhibition give rise to phenotypes of varying severity: short spindles, defective chromosome segregation, disorganized or absent telophase midbodies, spindle collapse and fused daughter nuclei. In addition, we noticed that nuclei originating from spindles with defective midbodies always gave rise to spindles with a very strong defective phenotype in the next mitotic cycle. The spindle collapse after Pav-KLP inhibition occurred at a later stage of mitosis than that observed after anti-KLP61F injection, which causes collapse at the

onset of the prometaphase-metaphase spindle elongation (Sharp et al., 2000; Brust-Mascher et al., 2009), suggesting that Pav-KLP plays an important role in maintaining pole-pole spacing. The observation that Pav-KLP inhibition prevented spindles from elongating during anaphase could reflect its role in stabilizing the ipMTs so that the necessary forces can be generated. These results are consistent with the hypothesis that Pav-KLP is involved in stabilizing the spindle structure, most probably by bundling ipMTs and providing a framework that allows other motor proteins to promote spindle elongation.

Defects in spindle morphogenesis after Pav-KLP inhibition were also consistently accompanied by the formation of interconnected adjacent spindles. Such connections have been observed after inhibition of KLP61F or KLP3A in an *ncd*-null mutant background (Sharp et al., 1999b; Kwon et al., 2004; Brust-Mascher et al., 2009); in this case, the spindle lacks two motors and is so disorganized that MTs splay outwards from the spindle and sometimes reach adjacent spindles. The consistent formation of interconnections after Pav-KLP inhibition supports the hypothesis that Pav-KLP is also involved in furrow assembly. Indeed, our data show that Pav-KLP not only colocalizes with actin at the cortex but is also responsible for actin remodeling: when Pav-KLP function was blocked, diminished furrow growth and loss of actin recruitment along the furrows were observed both in the syncytium and during cellularization.

We suggest that the role of Pav-KLP in spindle morphogenesis and membrane reorganization are distinct and can be explained by considering two Pav-KLP populations defined by the presence of the spindle envelope (Wolf, 1995). Inside the spindle envelope, Pav-KLP could function in spindle morphogenesis, whereas outside the spindle envelope it could function in membrane reorganization (Fig. 6C).

We observed that Pav-KLP is also involved in membrane and actin remodeling during cellularization, a process that is similar to conventional cytokinesis. During cellularization, loss of Pav-KLP function impedes both actin recruitment and membrane insertion into the furrow, thereby affecting the overall furrow length and organization. Modeling suggests that, during cellularization, Pav-KLP functions both as a force generator and a transporter by unfolding and pulling down membrane in the first, slow stage of furrow growth and transporting membrane vesicles to the furrow in the next, fast, stage of growth (Fig. 6A).

Pav-KLP might play a role in membrane and actin remodeling either via direct transport or via transport of factor(s) involved in actin regulation (Fig. 6). The interdependence between actin remodeling and membrane recruitment has been previously observed in *nuf* (Rothwell et al., 1998; Riggs et al., 2003), *dal* (Sullivan et al., 1993) and *dah* (Rothwell et al., 1999) mutants, and also in mutants containing the dominant-negative form of Rab11 (Pellissier et al., 2003), in which loss of actin localization and furrow-growth defects were observed. We observed that, in embryos expressing GFP-Nuf, loss of Pav-KLP function affected Nuf distribution. It has been shown that the centrosomal localization of Nuf relies on minus-end-directed dynein-mediated transport of Nuf along astral MTs from the periphery (Riggs et al., 2007). Here we suggest that Pav-KLP, as a plus-end motor, could be responsible for proper Nuf localization and actin recruitment to the cortex. Actin can be delivered to the furrows simply by being attached to the membrane vesicles, as is the case for Dah (Zhang et al., 2000). We were not able to determine whether Pav-KLP is responsible for the direct transport of actin to the cortex or whether it promotes the

delivery of signaling molecules. Polo kinase has been proposed as a signaling molecule that is required for centrosome function and cytokinesis, and that is transported by Pav-KLP (Adams et al., 1998). Using GFP-Polo-expressing embryos, we observed Polo localization to the cortex (data not shown), in addition to at centrosomes and the spindle midzone, similar to Pav-KLP localization. Our observations hint at a role for Pav-KLP in vesicle transport but more work is needed to elucidate the involvement of Pav-KLP in transport pathways in the early *Drosophila* embryo.

Altogether, our experimental work identified Pav-KLP as a stabilizing and transporting agent involved in both spindle and cortical dynamics. Furthermore, our quantitative modeling suggested a possible mechanical role for this motor as a force generator pulling down the membrane.

Materials and Methods

Fly stocks and embryo collection
Flies were maintained and embryos were collected as described (Sharp et al., 1999a). Experiments were performed using embryos expressing GFP-tagged myosin-II light chain, GFP-Nuf, GFP-Histone (all provided by William Sullivan, UCSC, Santa Cruz, CA), GFP-ROD (provided by Steven Henikoff, Fred Hutchinson Cancer Research Center, Seattle, WA), GFP-TUBULIN (provided by Tom Kaufman, Indiana University, Bloomington, IN) or GFP–Pav-KLP (provided by David M. Glover, University of Cambridge, Cambridge, UK).

Antibody production
The plasmid used for expressing the tail region of Pav-KLP fused to GST was generated as described previously (Kwon et al., 2004). Briefly, PCR-amplified Pav-KLP (nucleotides 2100-3056) encoding the tail domain was subcloned into pGEX-JDK (Amersham Pharmacia Biotech) and the corresponding bacterially expressed protein was purified on glutathione-agarose (Amersham Pharmacia Biotech). Two rabbit polyclonal antibodies against Pav-KLP were generated by immunization with purified Pav-KLP tail and were affinity purified on GST–Pav-KLP-tail columns. Antibodies were acid-eluted, neutralized in Tris buffer, dialyzed over night into PBS buffer plus 10 mM HEPES and then concentrated.

Drosophila embryo preparation
Microinjection of embryos 1-2 hours after fertilization was performed as described (Sharp et al., 2000; Kwon et al., 2004; Brust-Mascher and Scholey, 2009). Briefly, embryos were collected at 25°C for 1 hour, allowed to mature for 40 minutes, then dechorionated, placed on heptane glue, dehydrated for 3-6 minutes, covered with halocarbon oil and injected. As indicated for each experiment, Rhodamine-conjugated bovine tubulin, or Rhodamine-conjugated monomeric actin (Cytoskeleton, Denver, CO) was injected first and, after a 5-minute recovery period, embryos were injected with antibody. In some cases, GFP-tubulin-expressing embryos were directly injected with anti-Pav-KLP-tail antibodies at a needle concentration of 20-30 mg/ml. Controls were injected with buffer used to dilute antibody or tubulin.

S2 cells
Drosophila S2 cells were cultured as described (Morales-Mulia and Scholey, 2005) in Schneider medium (Invitrogen, Carlsbad, CA) supplemented with 10% heat-inactivated fetal bovine serum, 50 U/ml penicillin and 50 mg/ml streptomycin at 27°C. When needed, S2 cells were plated on concanavalin-A-coated coverslips and processed for immunofluorescence microscopy analysis as described (Morales-Mulia and Scholey, 2005). For Pav-KLP RNAi, an 894-bp fragment of *Pav-KLP* cDNA (nucleotides 1885-2779) was amplified using the following primers: 5′-TAATA-CGACTCACTATAGGGCACGAGAAGGAAAAGC-3′ and 5′-TAATACGACT-CACTA TAGGGGATTCAACTCCAAA GC-3′.

The PCR product was used as template for in vitro transcription using the Megascript T7 Kit (Ambion). *Drosophila* S2 cells were cultured at 27°C and treated with 30 μg/plate for 3 days.

Immunofluorescence and time-lapse microscopy
Fixation of *Drosophila* embryos for immunofluorescence was performed as described (Sharp et al., 1999a). For immunofluorescence analysis, rabbit anti-Nuf (gift from William Sullivan, UCSC, Santa Cruz, CA), rabbit anti-Pav-KLP, Rhodamine-conjugated goat anti-actin (Santa Cruz Biotechnology), FITC-conjugated anti-γ-tubulin monoclonal antibodies (Sigma-Aldrich) and propidium iodide for DNA were used. The appropriate secondary antibody (Jackson ImmunoResearch, West Grove, PA) was used.

For S2 cells, immunofluorescence-microscopy analysis was performed as described (Morales-Mulia and Scholey, 2005) with anti-γ-tubulin and anti-Pav-KLP antibodies.

Time-lapse images were acquired with an Olympus (Melville, NY) IX-70 inverted microscope equipped with an Ultra-View spinning disk confocal head (Perkin-

Elmer) and a UPlanApo 100× 1.35 numerical aperture (NA) or a PlanApo 60× 1.4-NA oil-immersion objective. Either a single confocal plane or a stack of 12 planes spaced by 0.5 μm were acquired at time intervals of 3-10 seconds at room temperature (20-22°C). Images were acquired with a Hamamatsu Orca II CCD camera. To follow cellularization, images were acquired on an Olympus FV1000 Laser Scanning Confocal with a 60× oil-immersion objective. All images were analyzed with MetaMorph Imaging software (Universal Imaging, West Chester, PA). Pole-to-pole distance as a function of time was measured from the position of the poles in each image. Calculations and statistical analyses were done on Microsoft Excel. S2-cell images are three-dimensional projections generated from stacks of eight sections (0.5-μm thick) using MetaMorph (Molecular Devices, Downingtown, PA).

Hydrodynamic assay
The molecular weight (MW) and subunit composition of Pav-KLP in embryo extracts were calculated using 5-20% sucrose gradient to estimate the S-value and analytical gel filtration FPLC (Hiprep Sephacryl S-300, GE) to determine the Stokes radius. Subunit MW was calculated from standard curves of relative mobility (Rm) vs log MW.

Computational model
We solved the model equations numerically using the *Virtual Cell* software (Slepchenko et al., 2002), with the initial conditions corresponding to a constant density of diffusing vesicles and zero density of transported vesicles. We assume a constant source of vesicles at the centrosome. We used the Dirichlet boundary conditions at the boundary of the centrosomal region, that is, the concentration of attached vesicles, C_{MT}, is equal to 1 there (vesicle density is normalized by the centrosomal density). At the right boundary corresponding to the furrow, absorbing boundary conditions are used. At all other domain boundaries, a no-flux boundary condition is used. The model parameters are listed in supplementary material Table S1. Parameter k is adjusted to fit the experimental data.

Supplementary material available online at
http://jcs.biologists.org/cgi/content/full/123/11/1862/DC1

References

Adams, R. R., Tavares, A. M. T., Salzberg, A., Bellen, H. J. and Glover, D. M. (1998). *pavarotti* encodes a kinesin-like protein required to organize the central spindle and contractile ring for cytokinesis. *Genes Dev.* **12**, 1483-1494.

Albertson, R., Riggs, B. and Sullivan, W. (2005). Membrane traffic: a driving force in cytokinesis. *Trends Cell Biol.* **15**, 92-101.

Albertson, R., Cao, J., Hsieh, T. S. and Sullivan, W. (2008). Vesicles and actin are targeted to the cleavage furrow via furrow microtubules and the central spindle. *J. Cell Biol.* **181**, 777-790.

Barmchi, M. P., Rogers, S. and Hacker, U. (2005). DRhoGEF2 regulates actin organization and contractility in the Drosophila blastoderm embryo. *J. Cell Biol.* **168**, 575-585.

Brust-Mascher, I., and Scholey, J. M. (2009). Microinjection techniques for studying mitosis in the Drosophila melanogaster syncytial embryo. *J. Vis. Exp.* **31**, doi: 10.3791/1382.

Brust-Mascher, I., Civelekoglu-Scholey, G., Kwon, M., Mogilner, A. and Scholey, J. M. (2004). Model for anaphase B: role of three mitotic motors in a switch from poleward flux to spindle elongation. *Proc. Natl. Acad. Sci. USA* **101**, 15938-15943.

Brust-Mascher, I., Sommi, P., Cheerambathur, D. K. and Scholey, J. M. (2009). Kinesin-5-dependent poleward flux and spindle length control in Drosophila embryo mitosis. *Mol. Biol. Cell* **6**, 1749-1762.

Cao, J., Alberson, R., Riggs, B., Field, C. M. and Sullivan, W. (2008). Nuf, a Rab11 effector, maintains cytokinetic furrow integrity by promoting local actin polymerization. *J. Cell. Biol.* **182**, 301-313.

Civelekoglu-Scholey, G., Sharp, D. J., Mogilner, A. and Scholey, J. M. (2006). Model of chromosome motility in Drosophila embryos: adaptation of a general mechanism for rapid mitosis. *Biophys. J.* **90**, 3966-3982.

Colombié, N., Cullen, C. F., Brittle, A. L., Jang, J. K., Earnshaw, W. C., Carmena, M., McKim, K. and Ohkura, H. (2008). Dual roles of Incenp crucial to the assembly of the acentrosomal metaphase spindle in female meiosis. *Development* **135**, 3239-3246.

Cytrynbaum, E. N., Scholey, J. M. and Mogilner A. (2003). A force balance model of early spindle pole separation in Drosophila embryos. *Biophys. J.* **84**, 757-769.

Cytrynbaum, E. N., Sommi, P., Brust-Mascher, I., Scholey, J. M. and Mogilner, A. (2005). Early spindle assembly in *Drosophila* embryos: role of a force balance involving cytoskeletal dynamics and nuclear mechanics. *Mol. Biol. Cell* **16**, 4967-4981.

Edgar, B. A., Odell, G. M. and Schubiger, G. (1987). Cytoarchitecture and the patterning of fushi tarazu expression in the Drosophila blastoderm. *Genes Dev.* **1**, 1226-1237.

Finger, F. P. and White, J. G. (2002). Fusion and fission: membrane trafficking in animal cytokinesis. *Cell* **108**, 727-730.

Foe, V. and Alberts, B. (1983). Studies of nuclear and cytoplasmic behavior during the five mitotic cycles that precede gastrulation in Drosophila embryogenesis. *J. Cell Sci.* **61**, 31-70.

Foe, V. E., Field, C. M. and Odell, G. M. (2000). Microtubules and mitotic cycle phase modulate spatiotemporal distributions of F-actin and myosin II in Drosophila syncytial blastoderm embryos. *Development* **127**, 1767-1787.

Fullilove, S. L. and Jacobson, A. G. (1971). Nuclear elongation and cytokinesis in Drosophila montana. *Dev Biol.* **26**, 560-577.

Glotzer, M. (2001). Animal cell cytokinesis.. *Annu. Rev. Cell Dev. Biol.* **17**, 351-386.

Glover, D. M. (2005). Polo kinase and progression through M phase in Drosophila: a perspective from the spindle poles. *Oncogene* **24**, 230-237.

Glover, D. M., Capalbo, L., D'Avino, P. P., Gatt, M. K., Savoian, M. S. and Takeda, T. (2008). Girds 'n' cleeks o' cytokinesis: microtubule sticks and contractile hoops in cell division. *Biochem. Soc. Trans.* **36**, 400-404.

Goshima, G. and Vale, R. D. (2005). Cell cycle-dependent dynamics and regulation of mitotic kinesins in Drosophila S2 cells. *Mol. Biol. Cell* **16**, 3896-3907.

Herant, M., Heinrich, V. and Dembo, M. (2005). Mechanics of neutrophil phagocytosis: behavior of the cortical tension. *J. Cell Sci.* **118**, 1789-1797.

Hickson, G. R., Hickson, G. R., Matheson, J., Riggs, B., Maier, V. H., Fielding, A. B., Prekeris, R., Sullivan, W., Barr, F. A. and Gould, G. W. (2003). Arfophilins are dual Arf/Rab 11 binding proteins that regulate recycling endosome distribution and are related to Drosophila nuclear fallout. *Mol. Biol. Cell* **14**, 2908-2920.

Inoue, Y. H., Savoian, M. S., Suzuki, T., Mathe, E., Yamamoto, M. T. and Glover, D. M. (2004). Mutations in orbit/mast reveal that the central spindle is comprised of two microtubule populations, those that initiate cleavage and those that propagate furrow ingression. *J. Cell Biol.* **166**, 49-60.

Kwon, M., Morales-Mulia, S., Brust-Mascher, I., Rogers, G. C., Sharp, D. J. and Scholey, J. M. (2004). The chromokinesin, KLP3A, dives mitotic spindle pole separation during prometaphase and anaphase and facilitates chromatid motility. *Mol. Biol. Cell* **15**, 219-233.

Lecuit, T. and Wieschaus, E. (2000). Polarized insertion of new membrane from a cytoplasmic reservoir during cleavage of the *Drosophila* embryo. *J. Cell Biol.* **150**, 849-860.

Mazumdar, A. and Mazumdar, M. (2002). How one becomes many: blastoderm cellularization in Drosophila melanogaster. *BioEssays* **24**, 1012-1022.

Minestrini, G., Harley, A. S. and Glover, D. M. (2003). Localization of Pavarotti-KLP in living *Drosophila* embryos suggests roles in reorganizing the cortical cytoskeleton during the mitotic cycle. *Mol. Biol. Cell* **14**, 4028-4038.

Mishima, M., Pavicic, V., Gruneberg, U., Nigg, E. A. and Glotzer, M. (2004). Cell cycle regulation of central spindle assembly. *Nature* **430**, 908-913.

Morales-Mulia, S. and Scholey, J. M. (2005). Spindle pole organization in Drosophila S2 cells by dynein, abnormal spindle protein (Asp), and KLP10A. *MBC* **16**, 3176-3186.

Neef, R., Klein, U. R., Kopajtich, R. and Barr, F. A. (2006). Cooperation between mitotic kinesins controls the late stages of cytokinesis. *Curr. Biol.* **16**, 301-307.

Nislow, C., Lombillo, V. A., Kuriyama, R. and McIntosh, J. R. (1992). A plus-end-directed motor enzyme that moves antiparallel microtubules in vitro localizes to the interzone of mitotic spindles. *Nature* **359**, 543-547.

Odell, G. M. and Foe, V. E. (2008). An agent-based model contrasts opposite effects of dynamic and stable microtubules on cleavage furrow positioning. *J. Cell Biol.* **183**, 471-483.

Papoulas, O., Hays, T. S. and Sisson, J. C. (2005). The golgin Lava lamp mediates dynein-based Golgi movements during Drosophila cellularization. *Nat. Cell Biol.* **7**, 612-618.

Pelissier, A., Chauvin, J.-P. and Lecuit, T. (2003). Trafficking through Rab11 endosomes is required for cellularization during *Drosophila* embryogenesis. *Curr. Biol.* **13**, 1848-1857.

Riggs, B., Rothwell, W., Mische, S., Hickson, G. R. X., Matheson, J., Hays, T. S., Gould, G. W. and Sullivan, W. (2003). Actin cytoskeleton remodeling during early *Drosophila* furrow formation requires recycling endosomal components Nuclear-fallout and Rab11. *J. Cell Biol.* **163**, 143-154.

Riggs, B., Fasulo, B., Royou, A., Mische, S., Cao, J., Hays, T. S. and Sullivan, W. (2007). The concentration of Nuf, a Rab11 effector, at the microtubule-organizing center is cell cycle-regulated, dynein-dependent, and coincides with furrow ormation. *Mol. Biol. Cell* **18**, 3313-3322.

Rosenblatt, J., Cramer, L. P., Baum, B. and McGee, K. M. (2004). Myosin II-dependent cortical movement is required for centrosome separation and positioning during mitotic spindle assembly. *Cell* **117**, 361-372.

Rothwell, W. F., Fogarty, P., Field, C. M. and Sullivan, W. (1998). Nuclear-fallout, a Drosophila protein that cycles from the cytoplasm to the centrosomes, regulates cortical microfilament organization. *Development* **125**, 1295-1303.

Rothwell, W. F., Zhang, C. X., Zelano, C., Hsieh, T. and Sullivan, W. (1999). The Drosophila centrosomal protein Nuf is required for recruiting Dah, a membrane associated protein, to furrows in the early embryo. *J. Cell Sci.* **112**, 2885-2893.

Royou, A., Field, C., Sisson, J., Sullivan, W. and Karess, R. (2004). Reassessing the role and dynamics of nonmuscle myosin II during furrow formation in early Drosophila embryos. *Mol. Biol. Cell* **15**, 838-850.

Scholey, J. M., Brust-Mascher, I. and Mogilner, A. (2003). Cell division. *Nature* **422**, 746-752.

Selser, J. C., Yeh, Y. and Baskin, R. J. (1976). A light-scattering characterization of membrane vesicles. *Biophys. J.* **16**, 337-356.

Sharp, D. J., McDonald, K. L., Brown, H. M., Matthies, H. J., Walczak, C., Vale, R. D., Mitchison, T. J. and Scholey, J. M. (1999a). The bipolar kinesin, KLP61F, cross-links microtubules within interpolar microtubule bundles of *Drosophila* embryonic mitotic spindles. *J. Cell Biol.* **144**, 125-138.

Sharp, D. J., Yu, K. R., Sisson, J. C., Sullivan, W. and Scholey, J. M. (1999b). Antagonistic microtubule-sliding motors position mitotic centrosomes in *Drosophila* early embryos. *Nat. Cell Biol.* **1**, 51-54.

Sharp, D. J., Brown, H. M., Kwon, M., Rogers, G. C., Holland, G. and Scholey, J. M. (2000). Functional coordination of three mitotic motors in Drosophila embryos. *Mol. Biol. Cell* **11**, 241-253.

Sisson, J. C., Field, C., Ventura, R., Royou, A. and Sullivan, W. (2000). Lava lamp, a novel peripheral golgi protein, is required for Drosophila melanogaster cellularization. *J. Cell Biol.* **151**, 905-918.

Slepchenko, B. M., Schaff, J. C., Carson, J. H. and Loew, L. M. (2002). Computational cell biology: spatiotemporal simulation of cellular events. *Annu. Rev. Biophys. Biomol. Struct.* **31**, 423-441.

Somers, W. G. and Saint, R. (2003). A RhoGEF and Rho family GTPase-activating protein complex links the contractile ring to cortical microtubules at the onset of cytokinesis. *Dev. Cell* **4**, 29-39.

Somma, M. P., Fasulo, B., Cenci, G., Cundari, E. and Gatti, M. (2002). Molecular dissection of cytokinesis by RNA interference in *Drosophila* cultured cells. *Mol. Biol. Cell* **13**, 2448-2460.

Strickland, L. I. and Burgess, D. R. (2004). Pathways for membrane trafficking during cytokinesis. *Trends Cell Biol.* **14**, 115-118.

Sullivan, W., Fogarty, P. and Theurkauf, W. (1993). Mutations affecting the cytoskeletal organization of syncytial Drosophila embryos. *Development* **118**, 1245-1254.

Ullrich, O., Reinsch, S., Urbe, S., Zerial, M. and Parton, R. G. (1996). Rab11 regulates recycling through the pericentriolar recycling endosomes. *J. Cell Biol.* **135**, 913-924.

Valentine, M. T., Fordyce, P. M., Krzysiak, T. C., Gilbert, S. P. and Block. S. M. (2006) Individual dimers of the mitotic kinesin motor Eg5 step processively and support substantial loads in vitro. *Nat. Cell Biol.* **8**, 470-446.

Warn, R. M. and Magrath, R. (1983). F-actin distribution during the cellularization of the Drosophila embryo visualized with FL-phalloidin. *Exp Cell Res.* **143**, 103-114.

Warn, R. M. and Robert-Nicoud, M. (1990). F-actin organization during the cellularization of the Drosophila embryo as revealed with a confocal laser scanning microscope. *J. Cell Sci.* **96**, 35-42.

Warn, R. M., Bullard, B. and Magrath, R. (1980). Changes in the distribution of cortical myosin during the cellularization of the Drosophila embryo. *J. Embryol. Exp. Morphol.* **57**, 167-176.

Wolf, K. W. (1995). Spindle membranes and spindle architecture in invertebrates. *Micron.* **26**, 69-98.

Young, P. E., Pesacreta, T. C. and Kiehart, D. P. (1991). Dynamic changes in the distribution of cytoplasmic myosin during Drosophila embryogensis. *Development* **111**, 1-14.

Zhang, C. X., Rothwell, W. F., Sullivan, W. and Hsieh, T. (2000). Discontinuous Actin Hexagon, a protein essential for cortical furrow formation in *Drosophila*, is membrane associated and hyperphosphorylated. *Mol. Biol. Cell.* **11**, 1011-1022.

Supplemental Table: model parameters

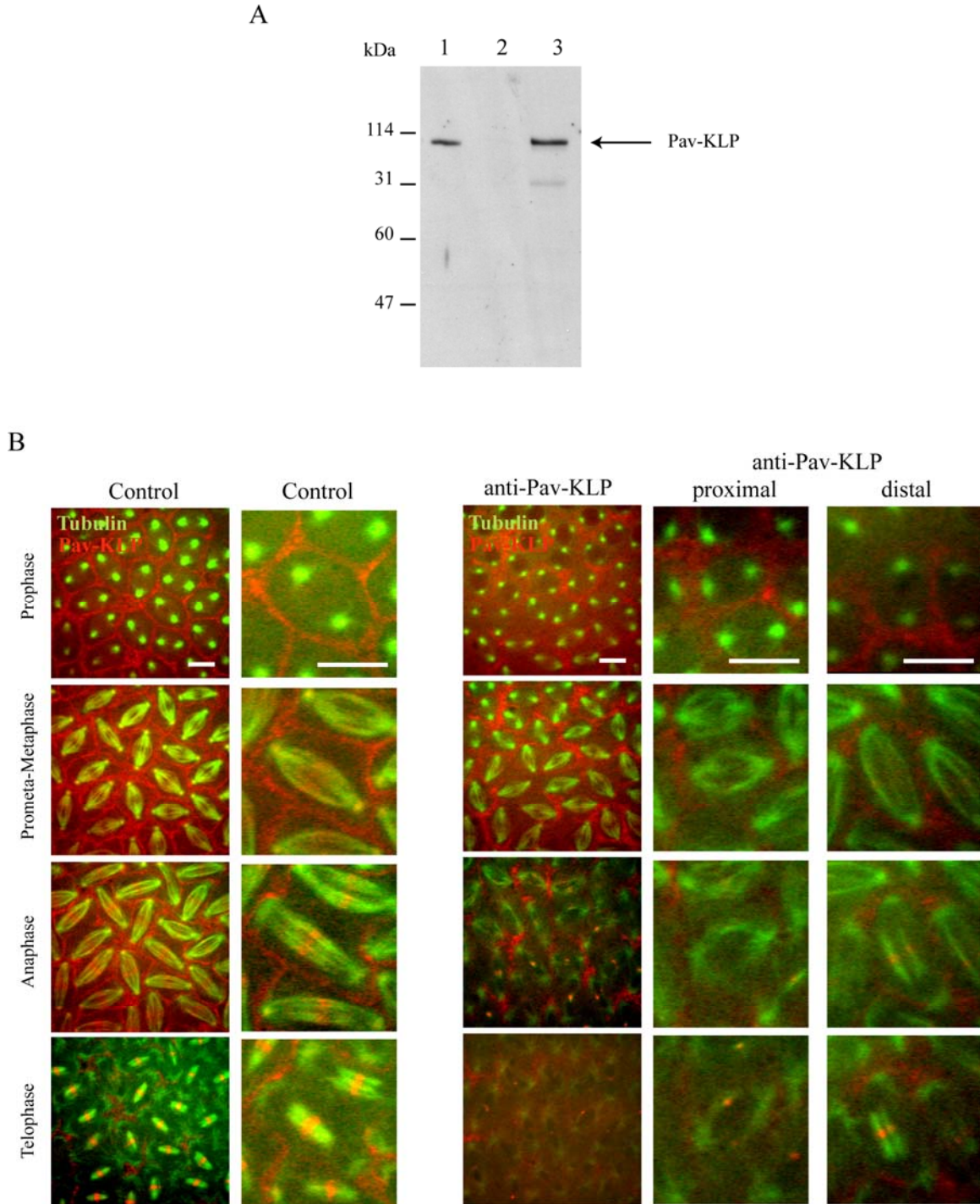| Description	Symbol	Value	Explanation/Reference
Diffusion constant	D	1 μm^2/s	Selser JC, Yeh Y, Baskin RJ. A light-scattering characterization of membrane vesicles. Biophys J. 1976 Apr;16(4):337-56.
Motor velocity	$|v|$	0.1 μm/s	Valentine MT, Fordyce PM, Krzysiak TC, Gilbert SP, Block SM. 2006. Individual dimers of the mitotic kinesin motor Eg5 step processively and support substantial loads in vitro. Nat Cell Biol. *8*:470-6.
Average microtubule length	L	5 μm	Cytrynbaum, E.N., J.M. Scholey, and A. Mogilner. 2003. A force balance model of early spindle pole separation in Drosophila embryos. Biophys J. *84*:757-69.
Attachment rate	k^0_{att}	1 sec^{-1}	Characteristic value for MT-based transport: Cytrynbaum, E.N., J.M. Scholey, and A. Mogilner. 2003. A force balance model of early spindle pole separation in Drosophila embryos. Biophys J. *84*:757-69.
Detachment rate	k_{det}	0.02 sec^{-1}	Chosen so that $1/k_{det} = L/|v|$ (see text)

Supplemental figures

Figure S1 Proper spindle organization requires correct Pav-KLP localization. (A) The anti-Pav-KLP antibody specifically recognizes the Pav-KLP polypeptide (~100 kD) in immunoblots. 0-2 h *Drosophila* embryonic high speed supernatant (HSS) (lane 1), AMPPNP supernatant (line 2) and MT pellet (lane 3) separated by SDS-7% PAGE and probed with the Pav-KLP antibody. In the presence of AMPPNP Pav-KLP is present only in the MT pellet and not in the supernatant. (B) Localization of Pav-KLP in the absence (left 2 columns) and presence (right 3 columns) of anti PavKLP antibody. All embryos were injected with rhodamine-tubulin. In each case a large field of view is shown on the left and individual spindles are shown on the right. After Pav-KLP inhibition, spindles that retain some protein are able to complete mitosis (distal region), while spindles without detectable PavKLP become disorganized and do not complete mitosis (proximal region)._Tubulin, green and Pav-KLP, red. Bars, 10 μm.
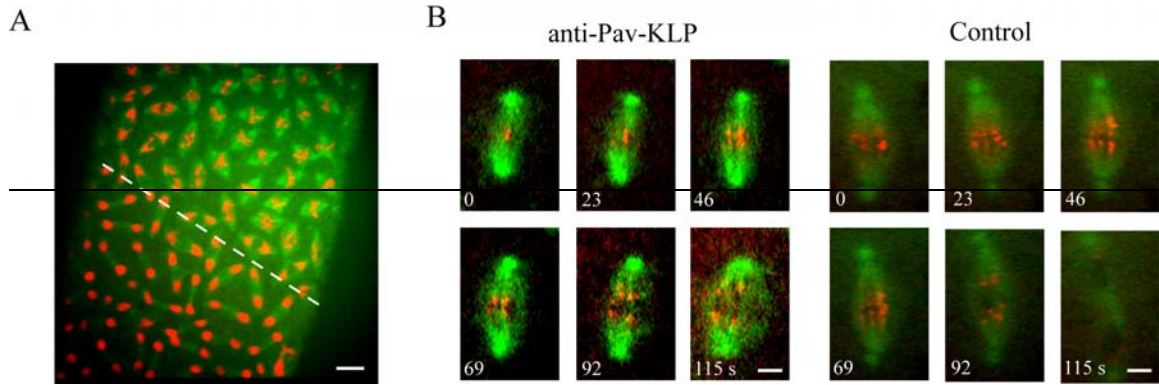
Figure S2 Effect of PavKLP inhibition on chromosome segregation. (A) Anti-PavKLP antibody injection into GFP-His expressing embryo causes a gradient of defects with the more severe ones next to the injection site (top of dotted line) and the less severe ones away from it (bottom of dotted line). In some cases, at the injection site, chromosomes did not complete segregation generating fused nuclei. Bar, 10 μm. (B) A representative spindle after PavKLP inhibition in a GFP-ROD expressing embryo (previously injected with rhodamine-tubulin) shows defects in kinetochore-to-pole movement and no anaphase elongation. Control spindle on right. We observed that kinetochores moved poleward at a slower rate (0.06±0.02 μm/sec in anti-PavKLP embryo vs 0.1±0.02 μm/sec in control). Bar, 2 μm. (ROD and His, red and Tubulin, green).
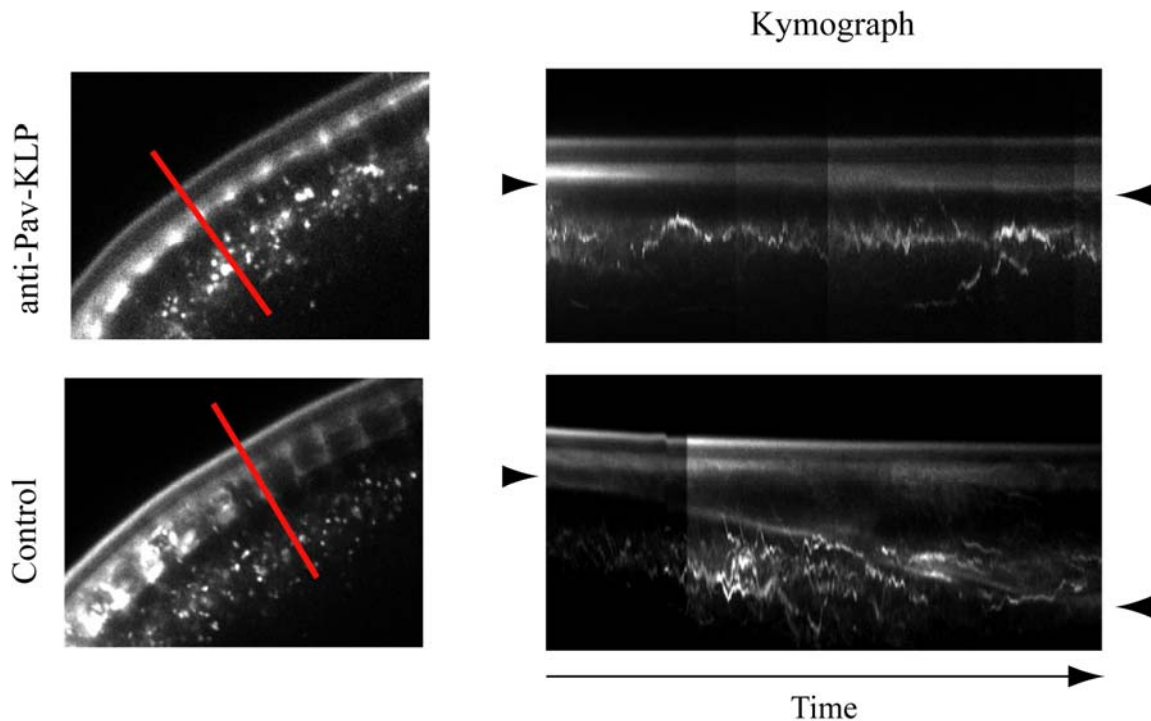

Figure S3 The cellularization of embryos requires Pav-KLP activity. Alexa Fluor WGA, injected into the peri-vitellin space was used as a cortical membrane marker. The growing membrane incorporates the injected fluorescent WGA making it easy to follow the membrane. Kymographs, taken during cellularization along the red lines, show normal membrane growth in control (bottom), but almost no growth in anti-Pav-KLP antibody injected embryos (top) Timecourse about 40 minutes. Arrowheads point to the membrane front at the start (left) and at the end (right). Some marker is internalized in vesicles, which move around and lead to irregular tracks in the kymographs.
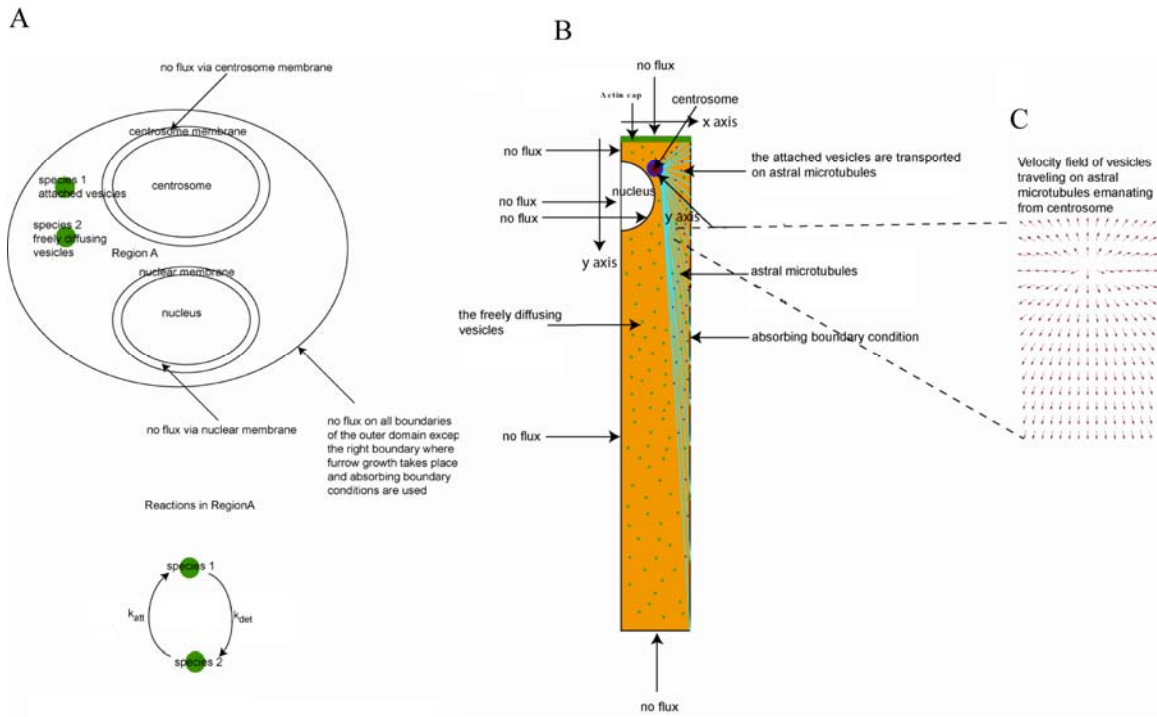
Figure S4 (A) Reactions used in the Virtual Cell model of furrow growth. (B) Schematic diagram of the geometry and boundary conditions used in the *Virtual Cell* model. (C) The velocity field for the MT-based vesicle transport.
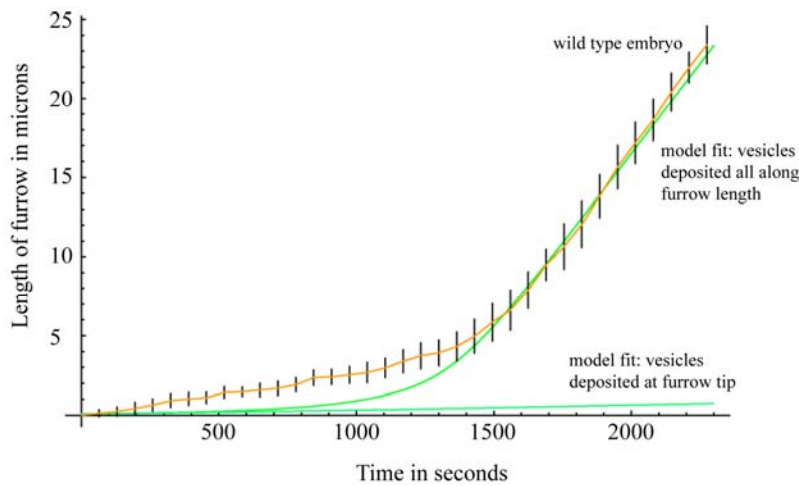

Figure S5 The model shows that vesicle deposition at the tip only does not fit the experimental data on furrow growth (orange curve). The model also shows that deposition all along the furrow length fits the later, fast phase well but not the initial, slow phase of growth: when the furrow is too short, too few MTs 'bump into' the furrow, and too few vesicles are delivered. In the later stage, when the furrow is very long, the MTs do not reach the basal end of the furrow, and the vesicles are mostly delivered into the apical part of the furrow at almost constant rate which explains the linear growth.
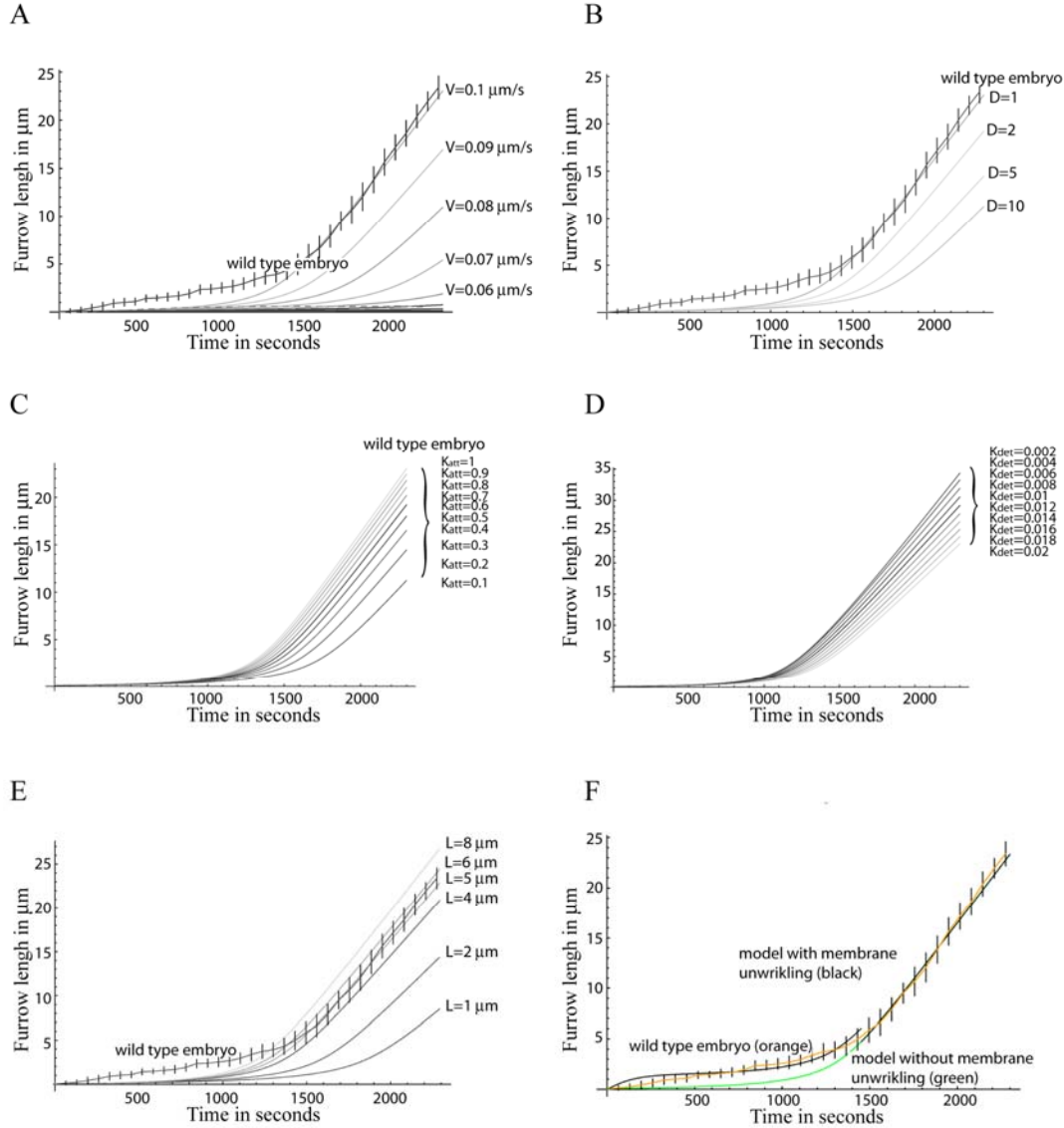
Figure S6 Effect of changing different parameters on furrow growth. The model parameters that determine furrow growth are the speed of transport $|v|$, the diffusion coefficient D, and the attachment and detachment rates of the motor, k^0_{att} and k_{det} respectively. In order to understand the effect of these parameters on furrow growth, we performed a parameter scan by varying one parameter at a time and keeping all others as listed in the table. (A) Effect of the motor velocity on furrow growth: A smaller transport speed leads to a smaller flux of attached vesicles at the furrow, and thus to slower furrow growth. The furrow growth is very sensitive to the transport speed: decreasing the speed by ~50% leads to an almost complete disappearance of furrow growth, in agreement with experimental observations in Pav-KLP inhibited embryos, i.e. no furrow growth during cellularization. The figure shows only variations of the speed down from 0.1 μm/sec because upward variations had only the obvious effect of accelerating transport, and because it is unlikely that molecular motors can accelerate, while they can easily be slowed down by physical obstacles. (B) Effect of the diffusion constant on furrow growth: decreasing it has no effect, so we do not show the results. Increasing the diffusion coefficient leads to vesicles dispersing more from the MTs when they detached resulting in a smaller flux of attached vesicles and a shorter furrow. However, even for this faster random mobility, the furrow growth is not very sensitive to the diffusion: increasing the diffusion constant by a factor of 10 decreases the growth rate by ~50% only. (C) Effect of the attachment rate on furrow growth: increasing this rate did not affect furrow growth (not shown); decreasing this rate had a small effect on furrow growth. (D) Effect of the detachment rate on furrow growth: We chose the detachment rate so that $1/k_{det} = L/|v|$ because at this detachment rate the vesicle has a significant probability of being delivered to the furrow before it detaches. Increasing the detachment rate slows down the transport tremendously, which was confirmed by our simulations (not shown). On the other hand, decreasing the detachment rate did not affect the furrow growth significantly. (E) Effect of the average MT length on furrow growth. In the realistic range of MT lengths > 4 μm, furrow growth is not very sensitive to the average MT length. (F) During the slow stage furrow growth can be explained by the force-limited unfolding of the wrinkled membrane.